Structural and Magnetic Study of $Sr_{3.3}Ca_{0.7}CoRh_2O_9$: A New Partially Ordered Antiferromagnetic System

M. Hernando,† K. Boulahya,† M. Parras,† A. Varela, J. M. González-Calbet,*,† and J. L. Martínez‡

Departamento de Química Inorgánica, Facultad de Ciencias Químicas, Universidad Complutense, E-28040, Madrid, Spain, and Instituto de Ciencia de Materiales, CSIC, Cantoblanco, E-28049, Madrid, Spain

Received April 4, 2002. Revised Manuscript Received July 3, 2002

The $\alpha = 3$, $\beta = 1$ term of the homologous series $(A_3A'BO_6)_\alpha(A_3B_3O_9)_\beta$ has been stabilized for the $Sr_{3.3}Ca_{0.7}CoRh_2O_9$ composition. The structural characterization by powder X-ray and electron diffraction and high-resolution electron microscopy indicates this material is isostructural to $Sr_4Ni_3O_9$. In this structure, two face-sharing octahedra alternate to one trigonal prism forming chains of one-dimensional polyhedra running parallel to the *c*-axis of a trigonal unit cell (*P*321) of parameters $a = 9.5767(7)$, $c = 7.9720(4)$ Å. The temperature dependence of the magnetic susceptibility of the $Sr_{3.3}Ca_{0.7}CoRh_2O_9$ is consistent with a weak antiferromagnetic interaction between magnetic cations. At low temperature our data seem to indicate the existence of a partially ordered magnetic state, as deduced from the small value of the magnetic part of the specific heat as well as the low entropy associated with the magnetic correlations.

Introduction

The structure of the 2H-ABO_3 hexagonal perovskite[1] can be regarded as formed by a hexagonal array of polyhedra chains, running parallel to the *c*-axis, formed by [BO_6] sharing-faces octahedra (O_h) (Figure 1a). The $A_3A'BO_6$ oxide shows the K_4CdCl_6[2] type which is constituted by the same hexagonal arrangement of the sharing-faces polyhedra chains, but now they are formed by the alternance of one [BO_6] octahedron and one [$A'O_6$] trigonal prism (TP) (Figure 1b). The structural similarity between the two structures[3] enables the formation of ordered intergrowths between them, leading to a very large family of one-dimensional oxides structurally related to the 2H-type.

From a structural point of view, all these 1D oxides can also be regarded as infinite polyhedra chains, constituted by octahedral and trigonal prism sharing faces. The different structures that can be generated by varying the octahedra/trigonal prism ratio, constitute the $(A_3A'BO_6)_\alpha(A_3B_3O_9)_\beta$ homologous series,[4] where A′ and B refer to metal cations in octahedral and trigonal prismatic environments, respectively. Variables α and β denote the number of structural blocks of the two end-oxides of the series, constituting every member of this family.

The study of the magnetic properties of low dimensional magnetic systems has been a subject of interest for a long time, and, among them, the above 1D system has attracted particular attention during the last few years, especially those materials exhibiting a transition to a 3D ordered state.[5,6] The compound $Ca_3Co_2O_6$[6] belongs to this kind of 1D-solid. This oxide corresponds to $\alpha = 3$, $\beta = 0$ term of the above-described 1D series, adopting the K_4CdCl_6 structure. Therefore, the basic network is an oriented hexagonal array of chains

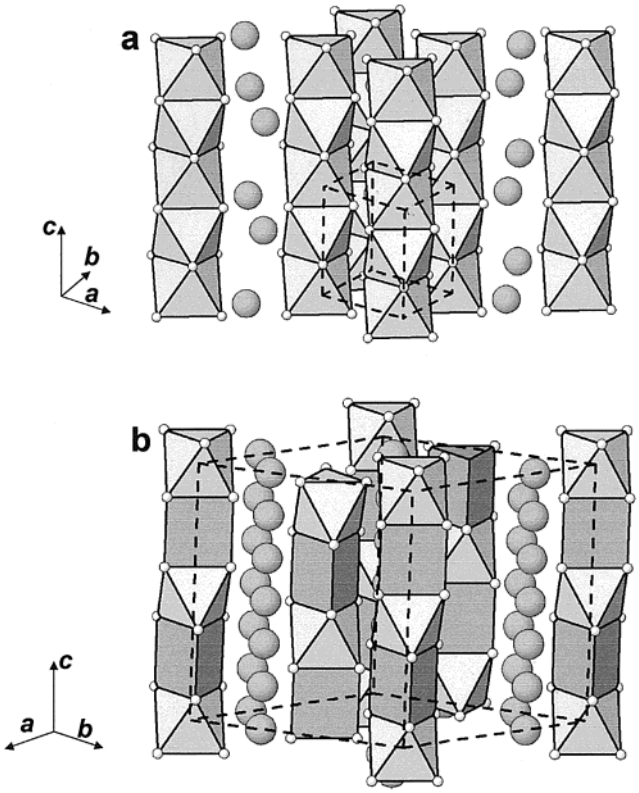

Figure 1. Structural models corresponding to 2H-ABO_3 (a) and K_4CdCl_6 (b).

* To whom correspondence should be addressed. Tel: 34913944342. Fax: 34913944352. E-mail: jgcalbet@quim.ucm.es.
† Universidad Complutense.
‡ Instituto de Ciencia de Materiales, CSIC.

(1) Lander, J. J. *Acta Crystallogr.* **1951**, *4*, 148.
(2) Bergerhoff, G.; Schmitz-Dumont, O. *Z. Anorg. Allg. Chem.* **1956**, *10*, 284.
(3) Darriet, J.; Subramanian, M. A. *J. Mater. Chem.* **1995**, *6*, 543.
(4) Boulahya, K.; Parras, M.; González-Calbet, J. M. *Chem. Mater.* **2000**, *12* (1), 25.

10.1021/cm0211756 CCC: $22.00
Published on Web 11/13/2002

constituted by alternating face-sharing [CoO_6] octahedra and [$CoO]_6$ trigonal prisms. The atomic spins in the chains are ferromagnetically coupled along the hexagonal *c*-axis forming a quasi-1D system. Interchain magnetic coupling is antiferromagnetic, and thus, there exists some degree of frustration in the ab plane triangular lattice. A ferrimagnetic 3D ordering is reached at temperatures below 13 K.[6−12]

When cobalt is partially substituted by rhodium, Ca_3CoRhO_6,[5] the crystal structure remains but the magnetic behavior is different. Ca_3CoRhO_6 is isostructural to $Ca_3Co_2O_6$, but the octahedral sites are now occupied by Rh atoms. Therefore, sharing faces CoO_6 trigonal prisms and RhO_6 octahedra, in a 1:1 ordered sequence, build up the 1D chains. From a magnetic point of view, the Ca_3CoRhO_6 exhibits the same triangular ferromagnetic spin arrangement; however, neutron diffraction studies[13] show that the Co/Rh-oxide realizes only a partially disordered antiferromagnetic (PDA) state at low temperature. In this state, $^2/_3$ of the ferromagnetic chains are ordered antiferromagnetically with each other and the remaining $^1/_3$ are left incoherent with the other chains.

In the A−Co−Rh−O system (A = alkaline-earth), only another 1D oxide has been reported. $Ba_8CoRh_6O_{21}$[14] is the $\alpha = 3, \beta = 5$ member of the above homologous series where the sharing-faces polyhedra are constituted by six [RhO_6] octahedra and one [CoO_6] trigonal prism. Such an oxide exhibits paramagnetic behavior over the whole temperature range. The high number of the octahedra [RhO_6], besides the bigger size of barium, should make the intrachain and interchain coupling more difficult, i.e., the short range order, thus avoiding 3D ordering. To study the influence of the O_h/TP ratio in the magnetic properties of this homologous series we have prepared a material with the composition $Sr_{3.3}Ca_{0.7}CoRh_2O_9$. This oxide corresponds to the $\alpha = 3, \beta = 1$ member of the above family, with $A_4CoRh_2O_9$ composition which, according to the structural arrangement of this series, should be formed by face sharing polyhedra constituted by two face sharing octahedra linked by one trigonal prism. The smaller size of the A cations together with the smaller O_h/TP ratio, enhances the magnetic cation coupling. So we would expect a magnetic behavior close to that of the $Ca_3Co_2O_6$ or Ca_3CoRhO_6 systems, i.e., coupling inside the chain and strong magnetic interactions between the chains.

Experimental Section

To isolate a $\alpha = 3, \beta = 1$ as a single phase, materials with different Ca/Sr ratios have been prepared. The best results are obtained for the Ca/Sr = 0.7/3.3 cationic ratio. A polycrystalline $Sr_{3.3}Ca_{0.7}CoRh_2O_9$ sample was prepared by solid-state reaction. Stoichiometric amounts of the corresponding Sr and Ca carbonates ($SrCO_3$, $CaCO_3$; Aldrich 99.99%), Co_3O_4 (Aldrich, 99.99%), and Rh_2O_3 (Aldrich 99.8%) were initially heated in air at 1173 K for 11 h in order to decompose the carbonates. Then, the sample was treated in air for 6 days at 1323 K with intermediate grindings.

The average cationic composition was determined by inductively coupled plasma-atomic emission spectrometry (ICP-AES) carried out in a Perkin Elmer 3300 DV. The local composition in every crystal was analyzed by X-ray energy dispersive spectroscopy (EDS). For this purpose, a JEOL 2000 FX electron microscope equipped with a LINK ISIS 300 analyzer system was employed. Chemical composition agrees with the experimental composition.

Powder X-ray diffraction (XRD) patterns were collected at room temperature on a Philips X'pert diffractometer with a graphite monochromator and using Cu Kα radiation. Data were collected in the angular range $5 \leq 2\theta/° \leq 100$ with a 2θ step size of 0.04° and counting time of 12 s/step. Diffraction data were analyzed by the Rietveld method[15] using the Fullprof program.[16]

Selected area electron diffraction (SAED) was carried out using a JEOL 2000FX electron microscope fitted with a double-tilting goniometer stage (±45°). High-resolution electron microscopy (HREM) was performed on a JEOL 4000EX electron microscope fitted with a double-tilting goniometer stage (±25°). Simulated HREM images were calculated by the multislice method using the MacTempas software package.

The resistivity was measured in the 2 to 400 K range by the four-probe method in a standard He cryostat, with a magnetic field up to 9 T. Magnetic behavior was measured by a SQUID magnetometer in a temperature range from 2 to 300 K, under a maximum applied magnetic field of 5 T and by using the physical properties measurement system (PPMS, Quantum Design) with fields up to 9 T. The specific heat was measured using a commercial heat-pulse calorimeter from Quantum Design, by means of the heat-pulse relaxation technique.

Results and Discussion

Structural Characterization. The powder X-ray diffraction pattern of $(Sr_{0.825}Ca_{0.175})_4CoRh_2O_9$ is shown in Figure 2. All maxima can be indexed on the basis of a trigonal unit cell of space group *P*321 and parameters $a = 9.5767(7)$, $c = 7.9720(4)$ Å.

The microstructural characterization, by SAED and HREM, confirms the stabilization of the $\alpha = 3, \beta = 1$ member in the A−Co/Rh−O system. The most relevant SAED patterns, taken along the [0001], [$1\bar{1}00$], and [$1\bar{2}10$] zone axes, are shown in Figure 3a, b, and c, respectively. In the [0001] reciprocal plane, reflections are distributed in a hexagonal array corresponding to a lattice parameter close to 9.6 Å. The features of the [$1\bar{1}00$] plane are also those corresponding to this 1D member, and, as in the previous SAED pattern, all reflections are visible in agreement with space group *P*321.

Besides, all maxima appearing in the SAED pattern along [$1\bar{2}10$] can be indexed also on the basis of the trigonal unit cell described above. Moreover, as we have previously reported, this reciprocal plane provides the

(5) Niitaka, S.; Kageyama, H.; Kato, M.; Yoshimura, K.; Kosuge, K. *J. Solid State Chem*. **1999**, *146*, 137.
(6) Fjellvåg, H.; Gulbrandse, E.; Aasland, S.; Oslen, A.; Hauback, B. *J. Solid State Chem*. **1996**, *124*, 190.
(7) Aasland, S.; Fjellvåg, H.; Hauback, B. *Solid State Commun*. **1997**, *101*, 187.
(8) Kageyama, H.; Yoshimura, K.; Kosuge, K.; Mitamura, H.; Goto, T. *J. Phys. Soc. Jpn*. **1997**, *66*, 1607.
(9) Kageyama, H.; Yoshimura, K.; Kosuge, K.; Azuma, M.; Takano, M.; Mitamura, H.; Goto, T. *J. Phys. Soc. Jpn*. **1997**, *66*, 3996.
(10) Maignan, A.; Michel, C.; Masset, A. C.; Martin, C.; Raveau, B. *Eur. Phys. J. B* **2000**, *55*, 3605.
(11) Martínez, B.; Laukhin, V.; Hernando, M.; Fontcuberta, J.; Parras, M.; González-Calbet, J. M. *Phys. Rev. B, Condens. Matter Mater. Phys.* **2001**, *64*, 012417.
(12) Raquet, B.; Baibich, M. N.; Broto, J. M.; Rakoto, H.; Lambert, S.; Maignan, A. *Phys. Rev. B, Condens. Matter Mater. Phys.* **2002**, *65*, 104442.
(13) Niitaka, S.; Yoshimura, K.; Kosuge, K.; Nishi, M.; Kakurai, K. *Phys. Rev. Lett*. **2001**, *87* (17), 1772021.
(14) Zur loye, H.-C.; Stitzer, K. E.; Smith, M. D.; El Abed, A.; Darriet, J. *Inorg. Chem*. **2001**, *40*, 5152.
(15) Rietveld, H. M. *J. Appl. Crystallogr*. **1969**, *2*, 65.
(16) Rodríguez-Carvajal, J. *Physica B* **1993**, *192*, 55.

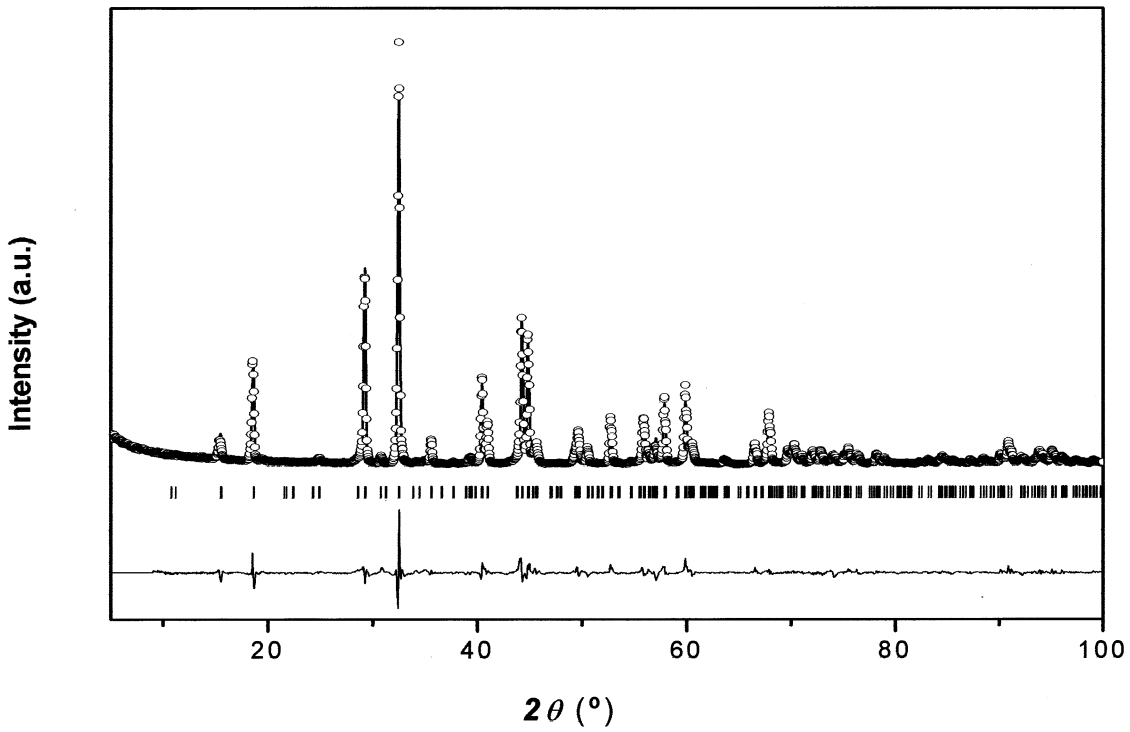

Figure 2. Graphic results of the fitting of the XRD pattern of $Sr_{3.3}Ca_{0.7}CoRh_2O_9$: experimental (points), calculated (solid line), and difference (bottom).

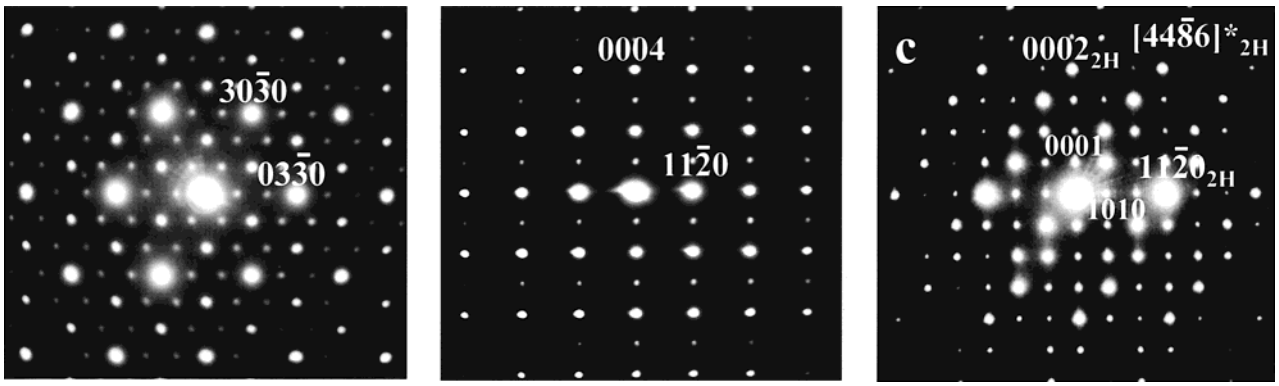

Figure 3. SAED patterns corresponding to $Sr_{3.3}Ca_{0.7}CoRh_2O_9$ along the [0001] (a), $[1\bar{1}00]$ (b), and $[1\bar{2}10]$ (c), zone axes.

α and β values, and thus, allows direct identification of the stabilized member. For this purpose, it is useful to consider the 1D phase as a modulated commensurable superstructure of the 2H-hexagonal type, whose planes appear in the SAED pattern as the most prominent spots (referred to as 2H in Figure 3c). The less intense ones correspond to the superstructure maxima, that follow the $[\alpha+\beta\ \alpha+\beta\ 2\alpha]^*_{2H}$ reciprocal direction.[4] As it can be observed, in this case, such a direction corresponds to $[44\bar{8}6]^*_{2H}$, i.e., confirming the stabilization of the $\alpha = 3$, $\beta = 1$ member for this Rh/Co oxide.

Figure 4 shows the high-resolution electron micrograph corresponding to $Sr_{3.3}Ca_{0.7}CoRh_2O_9$, along the $[1\bar{2}10]$ zone axis. An apparently well ordered material is observed with *d* spacings close to 8.3 and 8.0 Å corresponding to the d_{100} and d_{001}, respectively, of the above-mentioned unit cell. The image features are very close to that found in the isostructural compounds, $Sr_4Ni_3O_9$[17] or $(Ca_{0.5}Sr_{0.5})_4Co_3O_9$,[18] and can be interpreted in a similar way. The brightest dots are attributed to columns of metal atoms at trigonal prismatic sites and to the Ca/Sr atoms. It is worth stressing that two different parts can be distinguished in the image as a function of the thickness. The thickest area (zone A in the image) can be imaged as formed by bright dots forming linear triplets defining a rectangular configuration. Such a disposition is the expected for the $\alpha = 3$, $\beta = 1$ structure when projected along $[1\bar{2}10]$ (inset at figure). In fact, the simulated image, inset at zone A of figure, nicely fits with the experimental one for $\Delta t = 6$ nm and $\Delta f = -65$ nm values. In the thinnest area (marked B in the figure), it can be observed that two bright dots alternate with two less bright ones along the *c*-axis. Such a contrast variation can be associated with the ...1TP−$2O_h$−1TP... polyhedra sequence characteristic of the $A_4B_3O_9$ structure. The calculated image agrees with the experimental one for $\Delta t = 4$ nm and $\Delta f = -95$ nm values.

(17) Huvé, M.; Renard, C.; Abraham, F.; Van Tendeloo, G.; Amelinckx, S. *J. Solid State Chem.* **2000**, *135*, 1.

(18) Boulahya, K.; Parras, M.; González-Calbet, J. M. *J. Solid State Chem.* **1999**, *145*, 116.

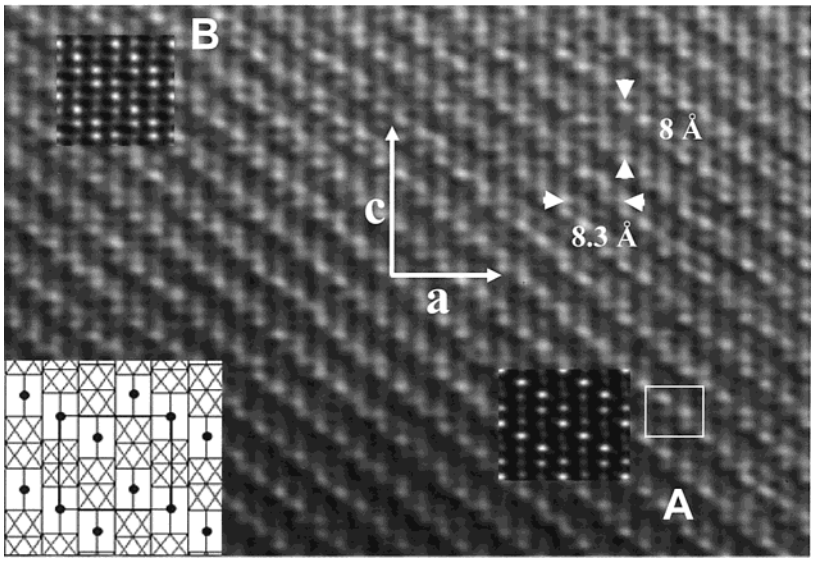

Figure 4. HREM image of $Sr_{3.3}Ca_{0.7}CoRh_2O_9$ along [1$\bar{2}$10]. The corresponding structural model, projected along the same direction, is included. Calculated images for zones A and B are shown in the inset.

Structure Refinement. The previous results suggest that 1D-$Sr_{3.3}Ca_{0.7}CoRh_2O_9$ adopts the structure corresponding to the $\alpha = 3$, $\beta = 1$ member; i.e., it is isostructural to $Sr_4Ni_3O_9$.[19] Therefore, the latter has been used as the starting model for the refinement of the XRD pattern. In this structure the Ni atoms are distributed over five crystallographic sites, two of which present trigonal prismatic coordination, while the other three correspond to octahedral oxygen environment. In our case, as a starting point, Sr and Ca have been considered as disordered over three crystallographic positions in the space group *P*321, and cobalt and rhodium atoms have been distributed in the trigonal prisms and the octahedral sites, respectively. However, during preliminary refinements, it became apparent that both transition metal cations are partially disordered, at least in some crystallographic positions. Therefore, the Co/Rh fractional occupancy, over the five crystallographic sites, was also included in the refinement. The observed, calculated, and difference diffraction profiles are shown in Figure 2. The final structural parameters are listed in Table 1. Table 2 shows some selected interatomic distances, which will be relevant for the discussion.

According to these results, Co and Rh atoms are distributed in the prismatic sites, although in a different ratio. In this sense, Co occupies approximately 75% and 60% of the trigonal prisms centered at (1/3 2/3 z) and (0 0 1/2), respectively. The remaining Co and Rh are disordered over the three crystallographically different octahedral sites, with the corresponding fractional occupation being included in Table 1. The cationic composition obtained from this refinement nicely fits with the experimental one.

The crystal structure (depicted in Figure 5) can be described as infinite 1D-chains formed by the ...1TP−$2O_h$−1TP... polyhedral sequence. The space between chains is occupied by the Sr/Ca metals that are coordinated to oxygen atoms at distances in the range 2.3−3.13 Å. The M(1), M(2), and M(3) oxygen environments define quite regular octahedra with average M−O distances corresponding to 2.05, 2.02, and 2.05 Å, for M(1), (2), and (3), respectively. All of these are consistent with previously reported bond-lengths in comparable rhodium-containing oxides, as $Ba_9Rh_8O_{21}$[20,21] (d_{Rh-O} = 2.03−2.23 Å), Ca_3CoRhO_6[5] (d_{Rh-O} = 2.003 Å), or in Ca_3-

Table 1. Final Structural Parameters of $(Sr/Ca)_4CoRh_2O_9$[a]

atom	*x*/*a*	*y*/*b*	*z*/*c*	occ.
Sr/Ca(1)	0.019(1)	0.687(1)	0.261(1)	1
Sr/Ca(2)	0.369(1)	0	1/2	1
Sr/Ca(3)	0.312(1)	0	0	1
M(1)	0	0	0.165(2)	Rh: 0.69(6)[b]
M(2)	1/3	2/3	0.065(2)	Rh: 0.67(6)[b]
M(3)	1/3	2/3	0.385(2)	Rh: 0.70(6)[b]
M(4)	0	0	1/2	Rh: 0.36(6)[b]
M(5)	1/3	2/3	0.707(2)	Rh: 0.24(6)[b]
O(1)	0.502(6)	0.664(6)	0.227(6)	1
O(2)	0.719(5)	0.208(6)	0.443(4)	1
O(3)	0.830(7)	0	0	1
O(4)	0.666(5)	0.169(4)	0.081(6)	1
O(5)	0.028(5)	0.190(5)	0.300(5)	1
				1

[a] S. G. *P*321 (164), $a = 9.5767(7)$ Å, $c = 7.9720(4)$ Å, $B_{overall}$ (Å^2)= 0.34(4). $R_B = 0.076$, $R_{wp} = 0.138$, $R_{exp} = 0.05$, $\chi^2 = 7.8$. [b] Tabulated values for M(1) to M(5) are fractional occupancies of Rh; Co fraction = 1 − Rh fraction.

Table 2. Selected Interatomic Distances (Å) in $(Sr/Ca)_4CoRh_2O_9$

Sr(1)−O(1)	2.63(6)	M(1)-O(1) × 3	2.07(6)
Sr(1)−O(1)	2.77(6)	M(1)-O(5) × 3	2.03(5)
Sr(1)−O(2)	2.45(5)	M(2)-O(1) × 3	2.07(6)
Sr(1)−O(2)	2.89(4)	M(2)-O(4) × 3	1.96(4)
Sr(1)−O(3)	2.55(2)	M(3)-O(1) × 3	2.07(6)
Sr(1)−O(4)	2.31(4)	M(3)-O(2) × 2	2.02(4)
Sr(1)−O(4)	3.13(5)	M(4)-O(5) × 6	2.30(4)
Sr(1)−O(5)	3.02(5)	M(5)-O(2) × 3	1.92(5)
Sr(1)−O(5)	2.38(5)	M(5)-O(4) × 3	2.30(4)
Sr(2)−O(1) × 2	2.60(5)	M(1)-M(1)	2.55(2)
Sr(2)−O(2) × 2	2.38(5)	M(2)-M(3)	2.57(2)
Sr(2)−O(2) × 2	2.95(5)	M(4)-M(1)	2.70(1)
Sr(2)−O(5) × 2	2.45(5)	M(5)-M(2)	2.85(2)
Sr(3)−O(1) × 2	2.47(5)	M(5)-M(2)	2.56(3)
Sr(3)−O(3) × 2	2.59(6)		
Sr(3)−O(4) × 2	2.84(3)		
Sr(3)−O(4) × 2	3.01(5)		
Sr(3)−O(5) × 2	2.73(4)		

(19) Abraham, F.; Minaud, S.; Renard, C. *J. Mater. Chem.* **1994**, *4*, 1763.

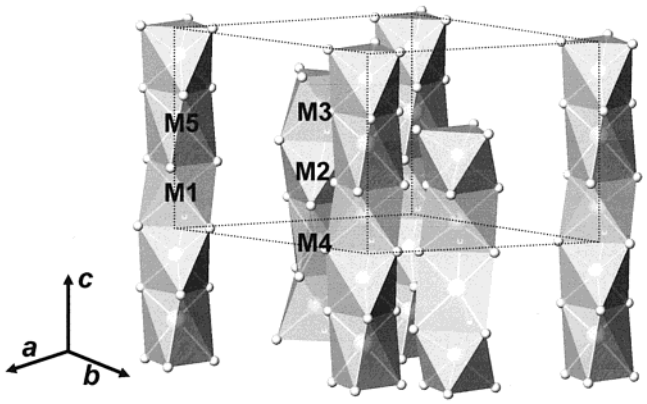

Figure 5. Schematic representation of the $Sr_{3.3}Ca_{0.7}CoRh_2O_9$ structure. Sr/Ca atoms have been omitted for clarity.

Co_2O_6[6] (d_{Co-O} = 2.06 Å). M(4) occupies the center of a regular oxygen trigonal prism, being coordinated at six oxygen atoms at 2.29 (Å). Such a M−O distance, although slightly longer, is comparable to those found for Co or Rh in the same oxygen polyhedron in $Ba_9Rh_8O_{24}$[20,21] (d_{Rh-O} = 2.2 Å) or Ca_3CoRhO_6[5] (d_{Co-O} = 2.149 Å). The M(5) polyhedron is less regular than the previous one, showing two different M−O distances, the average M−O distance, 2.17 Å, also in agreement with that reported above.

Inside the chains, interoctahedral M−M distances are comparable to that found for Rh−Rh in the same environment, in different oxides as in the hexagonal polytype 4H−$BaRhO_3$[22] (2.5−2.6 Å), or in the previously mentioned $Ba_9Rh_8O_{24}$ (d_{Rh-Rh}: 2.45−2.58 Å). The distances between metals in trigonal prism and in a neighboring octahedron sharing a trigonal face, are in the range between 2.56 and 2.85 Å, that can be compared to the $Rh_{(octahedral)}-Rh_{(trigonal\ prism)}$ (2.80 Å) and $Rh_{(octahedral)}-Co_{(trigonal\ prism)}$ (2.68 Å) distances corresponding to $Ba_9Rh_8O_{24}$ and Ca_3CoRhO_6, respectively.

Physical Properties. The resistivity was measured for a pellet sample as a function of temperature as presented in Figure 6. The temperature dependence of the resistivity is negative, indicating semiconducting behavior related to a localized system. The room-temperature value of the resistivity is 17 Ωcm. The data are very well fitted by the expression $\rho = A\exp(E_A/k_BT^{1/2})$, related to an activated variable range hopping model. The activation energy to achieve some conduction by hopping is 0.19 eV, as indicated by the slope in Figure 6. The application of an external magnetic field up to 9*T* does not modify the resistivity in the explored temperature range.

The magnetic susceptibility of $Sr_{3.3}Ca_{0.7}CoRh_2O_9$ versus temperature measured under field of 0.1*T* is shown in Figure 7. This picture shows the strong irreversibility between zero field cooled (ZFC) and field cooled (FC) branches of the susceptibility below 20 K (see inset). The magnetic susceptibility in the high-temperature range from 200 to 300 K can be fitted to the Curie−Weiss law,

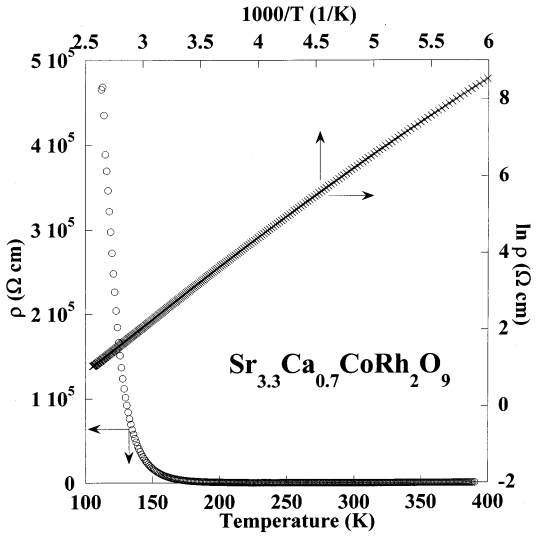

Figure 6. Temperature dependence of the resistivity for $Sr_{3.3}Ca_{0.7}CoRh_2O_9$. The ln$\rho$ vs 1/*T* is also included.

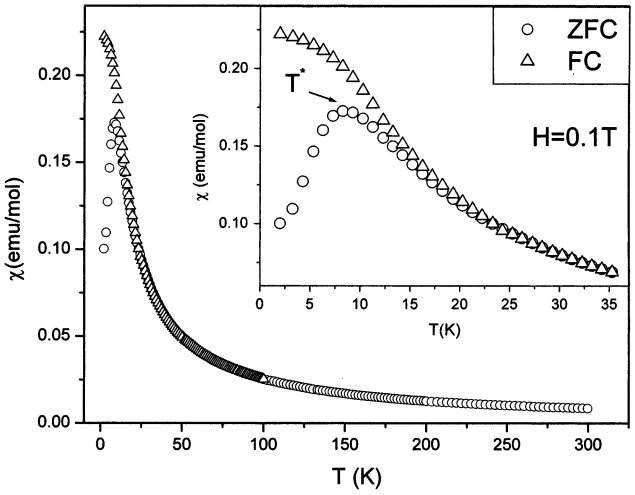

Figure 7. Susceptibility curves versus temperature corresponding to $Sr_{3.3}Ca_{0.7}CoRh_2O_9$ at $H = 0.1$ *T*. The detail of the low-temperature range showing the difference between ZFC and the FC branches of the susceptibility is shown in the inset.

leading to an extrapolated Weiss constant Θ = −14.7-(3) K, the paramagnetic effective Bohr-magneton number calculated corresponding to μ_{eff} = 2.68(1) μ_B/formula unit (f. u.). Between 150 and 50 K there is a positive deviation from Curie-like behavior followed by a large increase in the susceptibility ZFC measurement reaching a maximum at $T \sim 8.2$ K. The negative and small value of the Weiss constant (Θ = −14.7 K) can be indicative of a weak antiferromagnetic intrachain interaction, i.e., a weak exchange interaction integral. However, the existence of a competition between two different interactions that almost will cancel, i.e., ferro and antiferromagnetic between magnetic cations inside the chain, cannot be disregarded.

Note that the simplest distributions of the oxidation states of Rh and Co metals in a $A_4CoRh_2O_9$ composition correspond to: 1 Co^{II} and two Rh^{IV} or 1 Co^{III}, 1 Rh^{III}, and 1 Rh^{IV}, per f.u.. The μ_{eff} theoretical value expected for HS−Co^{II} and HS−Rh^{IV} is μ_{eff} = 2.22 μ_B/f. u., whereas that expected for HS−Co^{III}, LS−Rh^{III}, and HS−Rh^{IV} is μ_{eff} = 3.14 μ_B/f. u. The experimental value is intermedi-

(20) Stitzer, K. E.; Smith, M. D.; Darriet, J.; Zur loye, H.-C. *Chem. Commun*. **2001**, *17*, 1680.
(21) Boulahya, K.; Hernando, M.; Varela, A.; González-Calbet, J. M.; Parras, M.; Amador, U.; Martínez, J. L. *Eur. J. Inorg. Chem*. **2002**, 805.
(22) Chamberland, B. L.; Anderson, J. B. *J. Solid State Chem*. **1981**, *39*, 114.

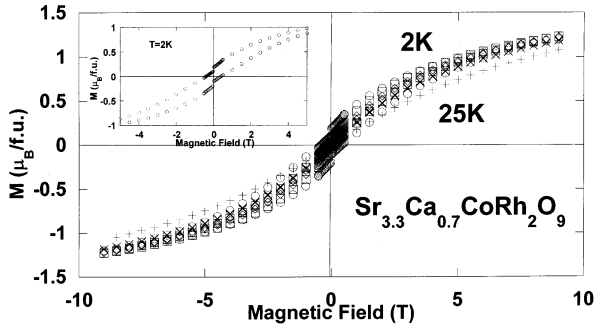

Figure 8. Magnetization curves versus applied field at several temperatures: 2, 5, 10, 15, and 25 K. The inset shows the details of the magnetization at 2 K for lower applied magnetic fields.

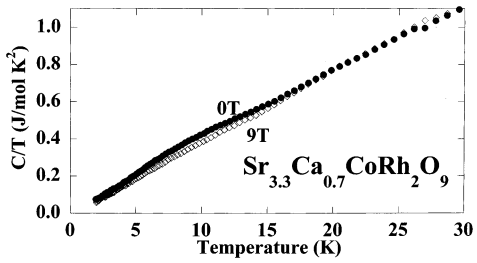

Figure 9. Temperature dependence of the specific heat of $Sr_{3.3}Ca_{0.7}CoRh_2O_9$ at 0*T* and 9*T*.

ate between these values suggesting an average oxidation state between both configurations.

To elucidate the origin of the magnetic anomaly observed at *T**, we have performed magnetization curves versus applied field at temperatures close to *T** in the range 2 to 25 K (Figure 8). As can be observed, the magnetization is increased suddenly by a field of a few hundreds of Gauss, followed by a very weak tendency to saturation at higher fields. This behavior is enhanced at $T = 2$ K (see inset). At this temperature the magnetization curve presents hysteresis. When the temperature increases the magnetization curves are progressively smeared out and the hysteresis disappears. This behavior could be connected with ferromagnetism or spin-glass behavior.[23] A long-range ferromagnetic ordering can be discarded because of the weak antiferromagnetic intrachain interactions, and, consequently, it seems that this compound presents a spin-glass state or a partially ordered magnetic state at low temperatures. Even if the system is clearly not saturated, the achieved saturated magnetization is only 0.75 μ_B/f. u. compared to 4 μ_B/f. u. obtained in $Ca_3Co_2O_6$ at 5 K and high magnetic field.[8]

The specific heat of $Sr_{3.3}Ca_{0.7}CoRh_2O_9$ is presented in Figure 9. The specific heat should have three different contributions in this temperature range: electronic, magnetic, and phononic. The first one will be negligible, because of the insulator character at low temperature presented in Figure 6. The phonon contribution will be difficult to calculate in this temperature range (2−40 K), because both models (Debye and Einstein) are usually valid at very low (Debye) or higher temperatures (Einstein oscillators). To extract the pure relative magnetic contribution to the specific heat, we repeat the same measurement at different applied magnetic fields up to 9 *T*. At high magnetic fields the variation of the entropy induced by the field will be very low (or spread in a very large temperature range). This can be seen in Figure 9, where the broad feature observed in a range from 3 to 20 K at zero field, disappears under a field of 9 *T*. From that data we could use the high field specific heat data as a background to remove all the phonons contributions. In this sense, a direct subtraction of both sets of data will give us the relative magnetic contribution to the specific heat. The results are presented in Figure 10, where a broad bump is observed centered at 8 K, with a clear shoulder at higher temperatures (20 K). The value of the magnetic specific heat is rather low, which will indicate a very disordered magnetic system. The temperature of the broad bump in the magnetic specific heat coincides very well with the maximum observed in the magnetic susceptibility, measured after zero field cooling process. In this sense, both experimental techniques are related to the same magnetic process.

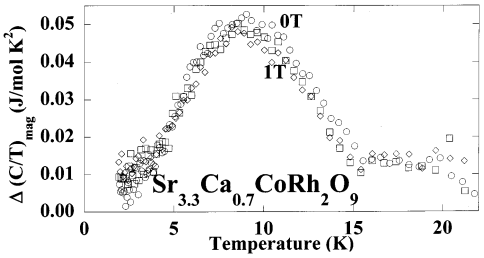

Figure 10. Temperature dependence of the magnetic specific heat after the subtraction of the phonon contribution for $Sr_{3.3}Ca_{0.7}CoRh_2O_9$.

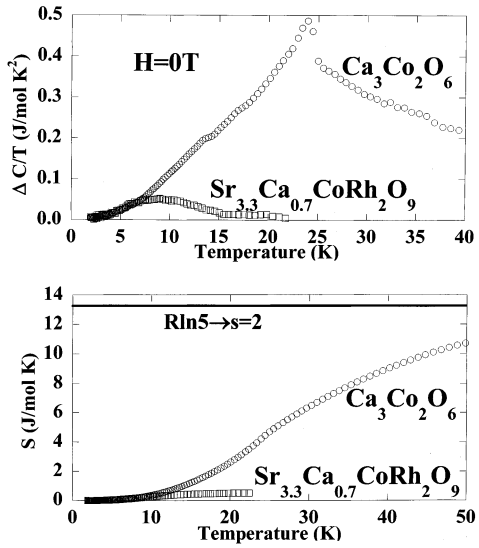

Figure 11. Comparison of the magnetic specific heat (a) and magnetic entropy (b) versus temperature for $Ca_3Co_2O_6$ and $Sr_{3.3}Ca_{0.7}CoRh_2O_9$.

To shed some light onto the magnetic disorder of this system, we have compared the above results with those obtained for the $\alpha = 3$, $\beta = 0$ member of the series with the composition $Ca_3Co_2O_6$. In this case, a long-range antiferromagnetic ordering between chains is achieved at $T_N = 24$ K, later a ferrimagnetic coupling between three chains is obtained at $T^* = 13$ K. The magnetic specific heat corresponding to the 1D compounds is presented in Figure 11a. For $Ca_3Co_2O_6$ a clear peak is

(23) Niaza, A.; Sampathkumaran, E. V.; Paulose, P. L.; Eckert, D.; Handstein, A.; Müller, K.-H. *Solid State Commun.* **2001**, *120*, 11.

observed at 24 K indicating the long range order. A broad bump is also observed at 13 K. By contrast, in $Sr_{3.3}Ca_{0.7}CoRh_2O_9$ the broad magnetic signal is centered at 8 K, and the intensity is very small compared to that of the former case. The integration of the magnetic specific heat, in the presented temperature range, is the magnetic entropy associated with the magnetic ordering. As observed in Figure 11b, in the case of $Ca_3Co_2O_6$ the entropy achieves the expected value corresponding to $s = 2$ ($R \ln(2S + 1)$). This value is related to one Co^{3+} in high spin state ($S = 2$), and another Co^{3+} in low spin state ($s = 0$). In the case of $Sr_{3.3}Ca_{0.7}CoRh_2O_9$ the entropy is by far much less, as a signature of a magnetic patially ordered system. According to these results, it seems that $Sr_{3.3}Ca_{0.7}CoRh_2O_9$ presents a partially ordered state, as observed in the lower term, $\alpha = 3$, $\beta = 0$, of this family, Ca_3CoRhO_6.[5] To our knowledge, this oxide constitutes the first example of an $\alpha = 3$, $\beta = 1$ term of the one-dimensional $(A_3A'BO_6)_\alpha(A_3B_3O_9)_\beta$ series showing such a behavior.

Acknowledgment. Financial support through research project MAT2001-1440 (CICYT, Spain) is acknowledged.

CM0211756